Simulations of ground effects on wake vortices at runways

By S. Eriksson † , M. Svärd ‡ AND J. Nordström ¶

1. Motivation and objectives

One of the factors limiting the capacity of airports is the hazard of remaining wake vortices on the runway. Wake vortices are generally two counter-rotating vortices coming off the wing tips of an aircraft. These vortices can remain on the runway for long periods with the risk of causing following planes to lose lift or tilt.

The basic physics of such a vortex pair is well understood. The circulation (or strength) Γ_0 of one vortex is given by

$$\Gamma_0 = \frac{W}{\rho U b s}\,, \qquad u_\theta(r) = \frac{\Gamma_0}{2\pi}\frac{r}{(r^2 + r_c^2)}\,, \qquad V_0 = \frac{\Gamma_0}{4\pi r_c}\,, \tag{1.1}$$

where W, U, b and ρ are the weight, landing speed, wing span of the aircraft and the density of air, respectively (see Figure 1). The non-dimensional parameter s is defined as $s = b_0/b$, b_0 being the distance between the vortices. If an elliptical lift distribution is assumed s is equal to $\pi/4$ (Coustols *et al.* (2006)).

Aircraft vortices can be modeled by cylinders of rotating air, which is a 2-D phenomenon. In the work of Winckelmans *et al.* (2006) the tangential velocity of a vortex $u_\theta(r)$ is defined as shown in Eq. 1.1, where r_c is the radius where the maximal velocity V_0 occur, i.e., $V_0 = u_\theta(r_c)$.

According to Winckelmans *et al.* (2006) a typical value of r_c is $0.05b_0$. Combining this with Eq. 1.1 results in a relation for the maximum tangential speed of the vortex, expressed as a function of the physical parameters of an aircraft:

$$V_0 = \frac{5W}{\pi\rho U b_0^2}\,. \tag{1.2}$$

Inserting numerical values for common aircraft leads to values of V_0 between $15-20$ m/s, which corresponds to a Mach number of 0.05. The Reynolds number is defined as $Re = V_0 \cdot r_c/\nu$, where ν is the kinematic viscosity. $Re = 5 \cdot 10^6$ would roughly correspond to air. However, the computational times for this Reynolds number become prohibitively expensive (see section 5) and hence in this report the Reynolds numbers considered range between 500 and $50,000$. (This could represent either a very viscous fluid or the air vortices generated by a model aircraft.)

The non-dimensional physical quantities (marked with *) used in this paper are defined

† Current Address: Department of Information Technology, Scientific Computing, Uppsala University, SE-75105 Uppsala, Sweden

‡ Current Address: Centre of Mathematics for Applications, University of Oslo, P.B 1053 Blindern N-0316 Oslo, Norway

¶ Current Address: Department of Information Technology, Scientific Computing, Uppsala University, SE-751 05 Uppsala, Sweden; Department of Aeronautical and Vehicle Engineering, KTH, The Royal Institute of Technology, SE-100 44 Stockholm, Sweden; Department of Computational Physics, FOI, The Swedish Defence Research Agency, SE-164 90 Stockholm, Sweden

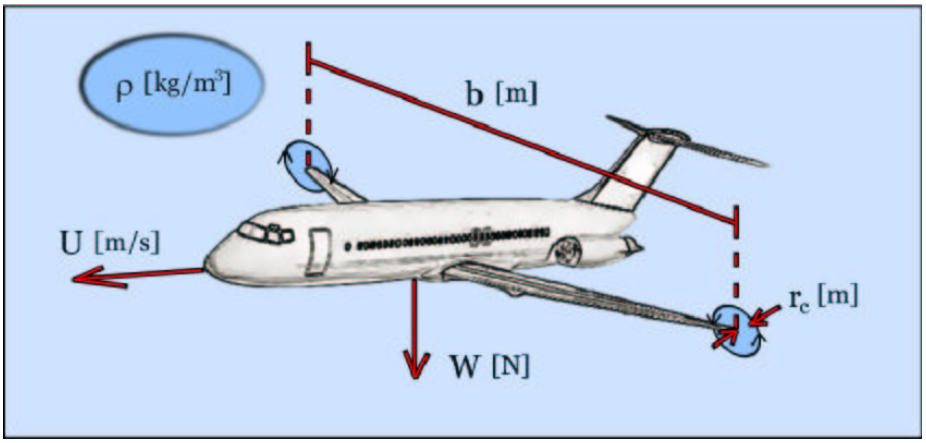

FIGURE 1. Physical parameters of an aircraft: Weight W, landing speed U, wingspan b. In addition: Radius of a vortex r_c, and the density of the air ρ.

as follows: The velocity $v^* = v/c$, c being the speed of sound (in air $c \approx 340m/s$ at sea level). The length $x^* = x/r_c$ and the non-dimensional time $t^* = t \cdot c/r_c$. $x^* = 20$ corresponds to the wingspan, and $t^* = 10,000$ represents approximately one minute.

2. Numerical method and grid generation

To produce the numerical results we use a provable stable, high-order finite difference method for the Navier-Stokes equations. The main theoretical feature of the method is the Summation-By-Parts (SBP) property combined with a penalty method (Simultaneous Approximation Term (SAT)) for imposing boundary conditions (see Gong & Nordström (2006), Carpenter *et al.* (1999), Mattsson & Nordström (2004), Svärd *et al.* (2007), Svärd & Nordström (2006)).

Besides making the boundary treatment stable, the SAT technique also provides information about the mesh resolution. For a mesh that is not sufficiently fine near the viscous wall, the no-slip boundary condition will not be obeyed to the desired accuracy, indicating that the mesh resolution needs to be increased.

The grid is important for the quality of the results. An optimal grid needs to have enough resolution in the regions of interest (it is coarser away from those regions). In the present study we stretch the grid using $\Delta y(i+1) = k \cdot \Delta y(i)$, where $k(i)$ is a suitable sum of smooth step functions

$$k(i) = 1 + A\frac{e^{(i-a)/m}}{e^{(i-a)/m} + e^{-(i-a)/m}} + B\frac{e^{(i-b)/m}}{e^{(i-b)/m} + e^{-(i-b)/m}} + ... \tag{2.1}$$

where $A, B, ...$ are the step sizes and $a, b, ...$ are the corresponding integer values for which the step should occur. The parameter m decides the smoothness of the steps. The grid can be easily regulated by changes in the coefficients $A, B, ..., a, b, ..., m$, and it is possible to vary the resolution near the wall boundary without significant changes in the rest of the grid. A similar formula was used in the x-direction, although adjusted to be symmetric, with a finer grid in the middle and a coarser grid toward the borders of the computational box. The number of grid points is 537 in the x-direction and 201, 225 or 257 in the y-direction, depending on the resolution near the ground. Figure 2 shows the near-wall region of the three grids considered.

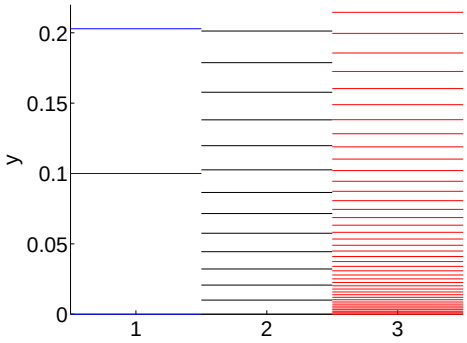

FIGURE 2. Horizontal grid lines of the three grids close to the ground. Left: $\Delta y_{min} = 0.1$. Center: $\Delta y_{min} = 0.01$. Right: $\Delta y_{min} = 0.001$. (At heights about $y \geq 5$ there is hardly any difference in coarseness between the grids.)

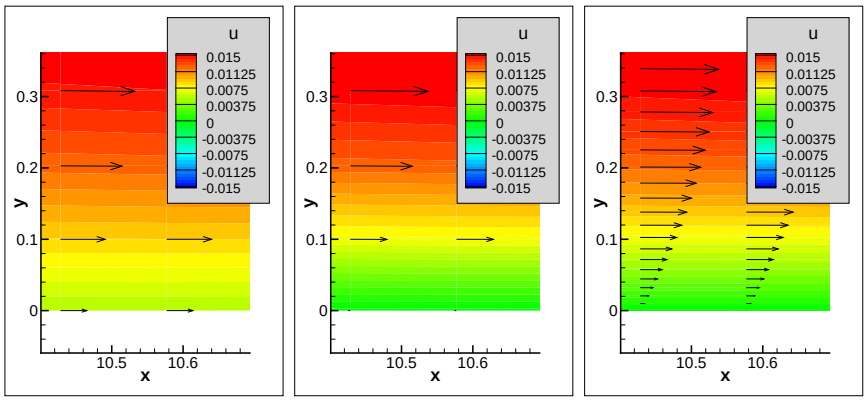

(a) Order (4,2) (b) Order (8,4) (c) Order (4,2)

FIGURE 3. Boundary layer under the right vortex at $t^* = 1000$, Re=500. Left: $\Delta y_{min} = 0.1$, order of scheme: (4,2). Middle: $\Delta y_{min} = 0.1$, order of scheme: (8,4). Right: $\Delta y_{min} = 0.01$, order of scheme: (4,2). In (b) and (c) the flow is sufficiently resolved.

3. Computations

The vortices are initiated by simply taking the average velocity field of one clockwise rotating vortex in position $[-10, 10]$, and one counter-clockwise rotating vortex in position $[10, 10]$ (Done using Eq. 1.1). Hence the vortex pair is initialized at the position $[\pm 10, 10]$, which corresponds to one wingspan in the x-direction and one half wingspan in the y-direction. The computational domain is $x \in [-60, 60]$ and $y \in [0, 40]$, which was considered sufficiently large to have no significant effects from the far-field boundary conditions. The maximum tangential velocity of each vortex is set such that it corresponds to a Mach number of 0.05 at the radius $r_c^* = 1$. The first Reynolds number, Re_V, is 500, which should roughly correspond to the value Re_Γ=Γ_0/ν=5000 used in Winckelmans *et al.* (2006).

This problem was computed with varying resolution in the boundary layer and schemes with different spatial accuracies. The following nomenclature is used to define the accuracy of a scheme. Spatial accuracy (a, b) means that the interior points are discretized with an accuracy of order a, while the boundary closure is carried out with order b. For example, the (8,4) scheme means that an eighth-order accurate scheme is used in the

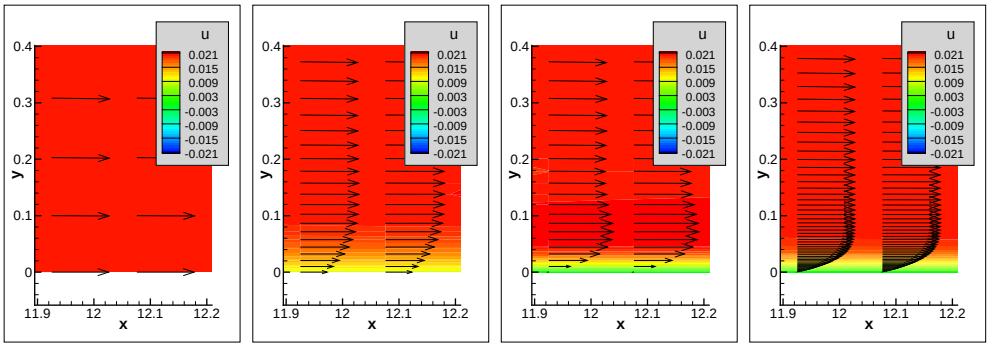

(a) Order (4,2) (b) Order (4,2) (c) Order (8,4) (d) Order (4,2)

FIGURE 4. Boundary layer under the right vortex at t=1000, Re=50,000. From left to right: (a) $dy_{min} = 0.1$, (4,2) order scheme. (b) $dy_{min} = 0.01$, (4,2) order scheme. (c) $dy_{min} = 0.01$, (8,4) order scheme. d) $dy_{min} = 0.001$, (4,2) order scheme.

interior and a fourth-order scheme on the boundary. Figure 3 shows the boundary layer below the right vortex. One can clearly see that in Figure 3(a) the grid is too coarse to make the x-component of the velocity vanish. However, this is a good example of how the penalty method gently forces the boundary condition from a Euler slip condition to a Navier-Stokes no-slip condition as the grid is refined. It is also a good example of how the resolution is improved as the order of the scheme is increased. As previously mentioned, both Fig. 3(b) and 3(c) indicate that the flow is resolved and that the particular meshes in these cases are sufficient. Hence the SAT technique can be a tool for deciding when the grid is fine enough.

In Fig. 4 the boundary layer for $Re = 50,000$ is shown, and in this figure it is even more evident that the boundary condition changes to a slip-wall boundary condition for the coarser grid, especially in Fig. 4(a) and 4(b).

To investigate the impact of the resolution of the boundary layer on the behavior of the vortices, the vortex trajectories corresponding to the velocity profiles in Fig. 3 are examined. These are shown in Fig. 5. The time integration scheme used is the standard four-stage Runge-Kutta scheme. The corresponding time step is chosen such that the temporal error is negligible relative to the error of spatial discretization. The difference between the trajectories is rather small for the different grids and accuracies, and all three solutions can be considered accurate enough to capture the important features of the flow. The trajectories of the computations for Re = 50,000 are shown in Fig. 6, which clearly shows that the resolution has a great impact on the vortex path.

As observed in Winckelmans *et al.* (2006) the solution computed using the Euler equations does not capture the rising of the vortices. Correspondingly, if the grid is too coarse the vortices cannot grip the ground and they simply roll away from each other, even if a no-slip boundary condition is implemented. As previously mentioned, resolution of the boundary layer is a good indication of whether the grid is sufficiently fine. By comparing the profiles for different Reynolds numbers, one observes for $Re = 500$, $\Delta y_{min} \approx 0.01$ is needed to capture the profile, and for $Re = 50,000$, $\Delta y_{min} \approx 0.001$ is necessary. This can be expected from the relation $\delta \sim 1/\sqrt{Re}$, where δ is the boundary layer thickness (see Kundu & Cohen (2004)).

The 2-D vorticity is $\omega = v_x - u_y$, where u is the x-component of the velocity and v the y-component. A clockwise-rotating vortex will have negative values of ω while counter-

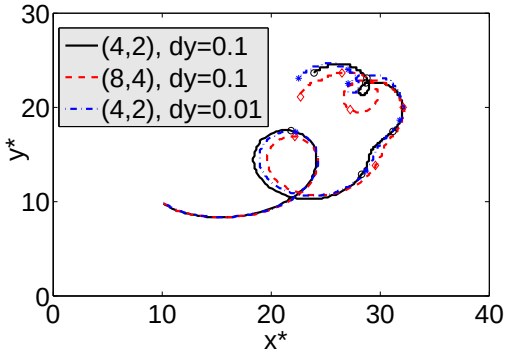

FIGURE 5. The trajectories of the right vortex for $Re = 500$. $\circ$, $\diamond$ and $*$ marks that time $t^* =$ 5000, 10,000, 15,000, 20,000, 25,000, 30,000.

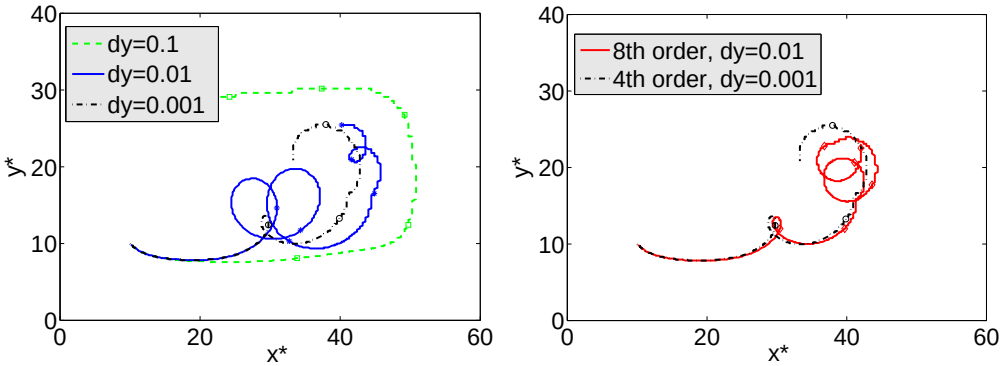

(a) (4,2) order scheme, different dy_{min}

(b) Comparison between (8,4) order on coarser grid with (4,2) order on fine grid.

FIGURE 6. The trajectories of the right vortex for Re=50,000.

clockwise rotating vortices have positive values. The creation of vorticity is shown in Fig. 7 . Vorticity is built up under the primary wing-tip vortices and as a consequence, they rise. The rather larger difference between the solution of different spatial accuracies is worth noting. On the same grid the (8,4) order scheme is capable of capturing much more detail in the flow than is possible for the (4,2) order scheme. To some extent the lower-order computation can catch the basic behavior of the vorticity field, but all the finer structures are lost. This result agrees with what was observed in the boundary profiles (see Fig. 4(b) and 4(c)).

These differences in detail actually have a significant effect on the trajectories of the vortex pair, which is clear from Fig. 6. From Fig. 6(b) another observation can be made: The (8,4) order scheme on a ten times coarser grid gives almost the exact same solution as the (4,2) order scheme on the finest grid up to time $\approx 12,000$. The behavior of the two curves then differ a bit from each other. Thus a fine grid is required not only close to the ground, but also in the inner part of the domain.

The desired Reynolds number is approximately $5 \cdot 10^6$, but in our computations the highest Reynolds number used is 50,000. The reason to choose a lower Re is that a calculation with approximately 100 times higher Re also requires *at least* a 10 times smaller

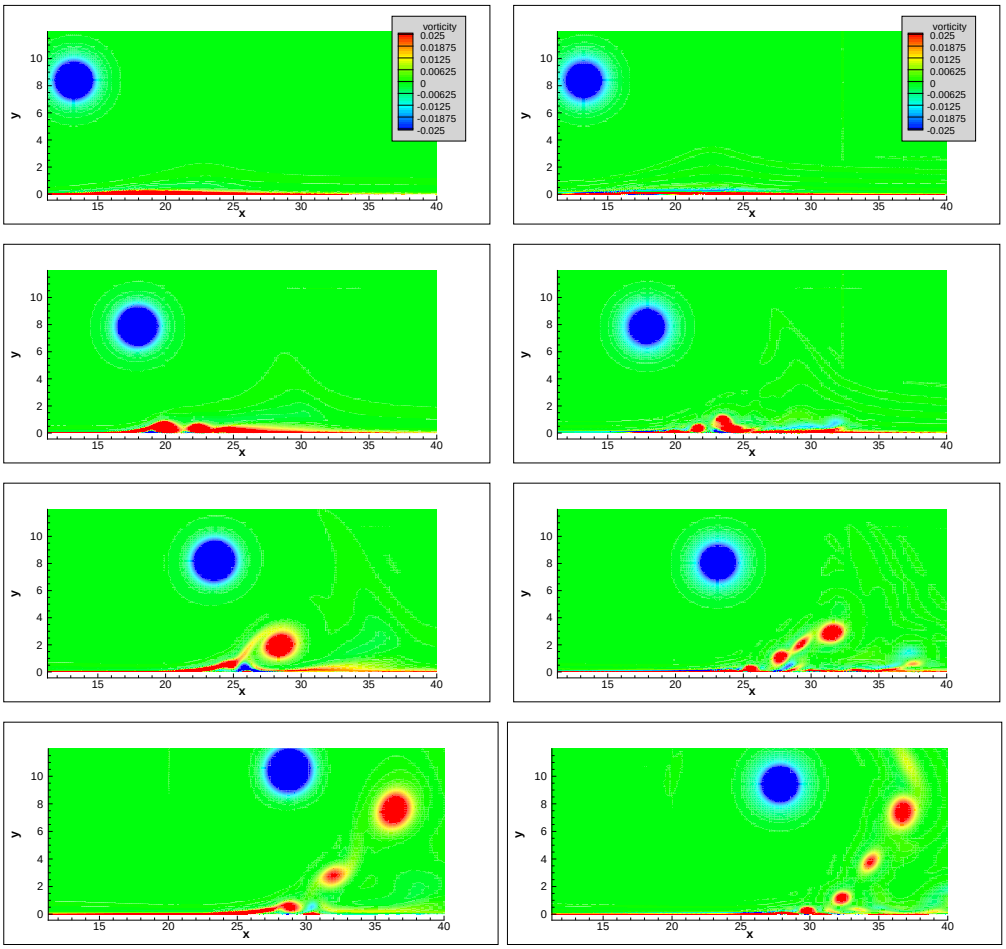

(g) Order of scheme: (4,2) (h) Order of scheme: (8,4)

FIGURE 7. The generation of secondary vortices under the right vortex for $Re = 50,000$ and $\Delta y_{min} = 0.01$, at t^*=1000, 2000, 3000 and 4000. On the left a (4,2) order scheme has been used, and on the right an (8,4) order scheme. This figure shows the negative 2-D vorticity ($-\omega$), i.e. blue indicates a counter-clockwise vortex and red indicates a clockwise vortex.

Δy_{min}, for the same order of the scheme. Also note that the time step is proportional to Δy_{min} for the explicit time integration schemes used in this work. Hence a realistic Reynolds number was not possible to compute because of the limited amount of available CPU power. The computations from Reynolds number 500 and 50,000 show that, for a higher Reynolds number, the trajectories of the vortex pair become much lower or flatter. An educated guess would be that for a very high Reynolds number, the trajectories would be even closer to the ground.

4. Computations in three dimensions

To verify the applicability of the 2-D calculations, a computation in 3-D was made. The grid used for the 3-D simulation had $\Delta y_{min} = 0.1$, i.e., the coarsest grid used in the 2-D runs. In addition there were 37 equidistant grid points added in the third (z)

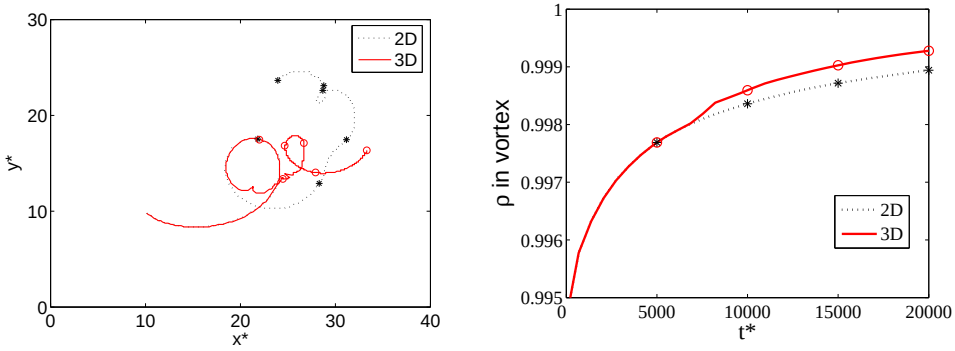

(a) The trajectories of the right vortex.

(b) Evolution of the density ρ^* at the center of the right vortex.

FIGURE 8. Re=500, $\Delta y_{min} = 0.1$, order (4,2). Comparison between 2-D and 3-D. $*$ and $\circ$ mark that time t^*= 5,000, 10,000, 15,000, 20,000, 25,000 and 30,000.

dimension. Hence the domain was [-60, 60] in x, [0, 40] in y, and [0, 5.4] in z-direction. The number of grid points was $537 \times 201 \times 37 \approx 4 \cdot 10^6$. At the ground ($y^*$=0) a no-slip BC was implemented, at the borders in x-direction (x^*=$\pm$60) and in the ceiling (y^*=40) a far-field BC (with the condition that the velocity should be zero) was used, and in z-direction periodic boundary conditions were implemented. The Reynolds number was 500, and as before the vortices were initialized in position (x, y)=[$\pm$10,10], but now for all z. Furthermore a random velocity field, of 1% of the top speed, was added in order to create some initial movement in the z-direction. If $R \in [-1, 1]$ (uniform random distribution) then

$$u_R = u + \frac{V_0^* \cdot R_u}{100}, \qquad v_R = v + \frac{V_0^* \cdot R_v}{100}, \qquad w_R = w + \frac{V_0^* \cdot R_w}{100}, \tag{4.1}$$

where u and v represent the original initial velocity field from the 2-D computations and $w = 0$ the original velocity in z-direction. In Fig. 8(a) the trajectory of the computation in 3-D is compared with the corresponding one in 2-D. The paths are very similar at the beginning, but at time $t^* \approx$7000 the vortices in the 3-D simulation start to behave differently.

The trajectory from the 3-D simulation is somewhat jagged, which is merely due to post-proccesing and hence not a real physical phenomenon. (Since the initial data has a small, random perturbation, the vortex position is sometimes found in the right vortex and sometimes in the left; this is why the path looks non-smooth in places.) More striking than the shakiness of the 3-D run is that the curves differ in position for $t^* > 7000$. Fig. 8(b) shows that a difference in the density occurs at the same time. (The density can be seen as measure of the strength: a strong vortex has a smaller density than a weak one. Far from the vortices the density is equal to one.) These results agree with those obtained by Winckelmans *et al.* (2006).

Note that even if the 2-D computation is not identical to its 3-D counterpart for simulation times longer than a couple of minutes (real time), it does lead to a worst-case estimate because the vortices are stronger and their paths are higher. The 2-D approximation is therefore a useful model.

In Fig. 9 the absolute value of the vorticity is shown as isosurfaces. Here one can see that at time $t^* = 3000$ the flow is essentially 2-D, since the vorticity still has a cylindrical

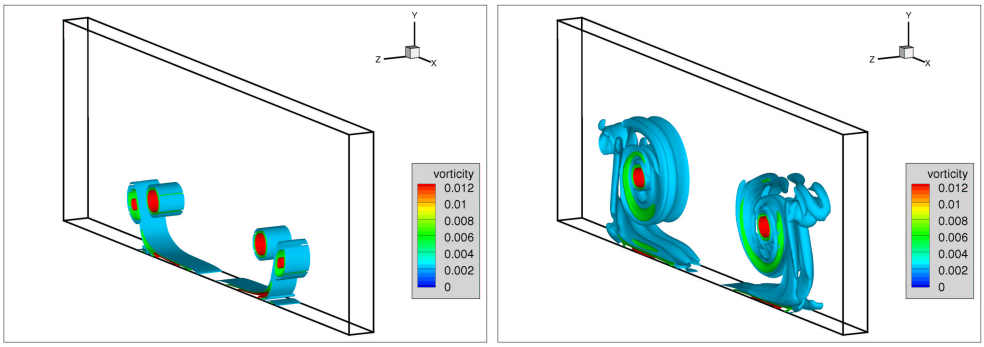

(a) t=3000 (b) t=12000

FIGURE 9. Isosurfaces of the vorticity. 3D simulation with $Re = 500$, $\Delta y_{min} = 0.1$ and 4,2 order of the scheme. The isosurfaces are $|\vec{\omega}| = 0.0025$, 0.006 and 0.0125

Re_V	Δy^*_{min}	grid points	proc.	acc.	Δt^*	time steps	CPU
Euler	10^{-1}	$1.08 \cdot 10^5$	8	4,2	0.142	$2.1 \cdot 10^5$	12:02:32
$5 \cdot 10^2$	10^{-1}	$1.08 \cdot 10^5$	8	4,2	0.138	$2.2 \cdot 10^5$	15:02:36
$5 \cdot 10^2$	10^{-1}	$1.08 \cdot 10^5$	8	8,4	0.138	$2.2 \cdot 10^5$	22:46:48
$5 \cdot 10^2$	10^{-2}	$1.21 \cdot 10^5$	16	4,2	0.014	$2.1 \cdot 10^6$	90:18:25
$5 \cdot 10^4$	10^{-2}	$1.21 \cdot 10^5$	8	4,2	0.018	$1.7 \cdot 10^6$	125:08:17
$5 \cdot 10^4$	10^{-2}	$1.21 \cdot 10^5$	16	8,4	0.018	$1.7 \cdot 10^6$	79:55:59

TABLE 1. CPU times (in hours) for some computations. The computations were parallelized and run on 8 or 16 processors. All examples here are in 2-D.

shape. At time $t^* = 12,000$ it is clear that the z-direction makes a difference since the cylinders now have turned into curved tubes.

5. Computer performance and full-scale simulations

The computations in this project were performed on a cluster of AMD Opteron processors with 1 GB RAM. Table 1 shows CPU times for some of the simulations performed during this project, with final $t^* = 30,000$. From this we can compute average computational times for the runs. For example, the time needed to do one time step when having $1.2 \cdot 10^5$ grid points distributed on 16 processors is $0.15s$ with (4,2) order of the scheme, and $0.17s$ with (8,4) order of the accuracy (compare lines 4 and 6 in Table 1). Note that even if a computation with a higher-order scheme takes longer than with lower ones (approximately 30−40% longer when going from (4,2) to (8,4)) it is not expensive compared to doing mesh refinement since Δt^* is dependent on Δy^*_{min}.

How much computational time is needed to perform simulations with realistic Reynolds numbers? Table 2 shows an estimate of the required CPU times for a full-scale simulation, based on the lower Re simulations from Table 1. The relation CPU$\sim$ [grid points]/($\Delta t \cdot$ [processors]) has been used, as well as the assumption that $\Delta y_{min} \sim 1/\sqrt{Re}$. The last

Re_V	Δy^*_{min}	grid points	processors	accuracy	Δt^*	CPU
$5 \cdot 10^2$	$1 \cdot 10^{-1}$	$1 \cdot 10^4$	10	8,4	0.15	1 hour
$5 \cdot 10^4$	$1 \cdot 10^{-2}$	$1 \cdot 10^6$	10	8,4	0.015	2 months
$5 \cdot 10^6$	$1 \cdot 10^{-3}$	$1 \cdot 10^8$	10,000	8,4	0.0015	2 months

TABLE 2. Estimated CPU times for some possible future 2-D simulations.

row in Table 2 predicts that a real-case simulation in 2-D would take two months on 10,000 processors.

The resulting two months of CPU time could (and should) be improved by the use of an efficient implicit time integration solver. We consider this to be a task for the future.

6. Summary and conclusions

Two- and three-dimensional computations of vortex pairs have been carried out using high-order finite difference schemes. The 2-D calculations were made for Reynolds numbers of 500 and 50,000. The purpose of these computations was to investigate the behavior of vortices interacting with the ground, and the effect of the Reynolds number on the flow field. The grid resolution and the accuracy of the spatial discretization were also varied to find the requirements for a properly resolved flow. The correlation between 2-D and 3-D simulation was investigated, and also it was concluded that the 2-D approximation is a useful model for the 3-D case.

The basic behavior of the wing tip vortex pair is as follows: They first interact and haul each other downward. When they approach the ground they start to build up reversed vorticity along the ground. The vortices start to roll away from each other close to the ground, but as soon as enough secondary vorticity has been built up, the vortices are forced to rise again. (This is a viscous effect; for a Euler simulation the vortices do not rise.) The tendency was that for the higher Re, the paths of the vortices were flatter (do not rise as fast) than for the lower Re.

The computational times required for our low-to-medium Reynolds number well-resolved simulations indicates that it is possible to carry out a full-scale simulation in a reasonable amount of time. The main requirement is that a massive number (thousands) of processors are available.

Acknowledgments

We thank Professor Parviz Moin, for making this project possible.

REFERENCES

CARPENTER, M. H., NORDSTRÖM, J., & GOTTLIEB, D. 1999 A stable and conservative interface treatment of arbitrary spatial accuracy. *J. of Comp. Phys.* **148**, 341−365.

COUSTOLS, E., ELSENAAR, A., DE BRUIN, A., WINCKELMANS, G., JACQUIN, L., LAPORTE, F., & SCHRAUF, G. 2006 Wake vortex alleviation studies and prospects.

Wake Vortex Research Needs for Improved Wake Vortex Separation Ruling and Reduced Wake Signatures, Part II - Specialist's Reports.

Gong, J. & Nordström, J. 2006 Stable, accurate and efficient interface procedures for viscous problems. *Technical Report 2006-019, april 2006, Uppsala University, Sweden.*

Kundu, P. K. & Cohen, I. M. 2004 Fluidmechanics, third edition. *Elsevier Academic Press, San Diego, California*

Mattsson, K. & Nordström, J. 2004 Summation by parts operators for finite difference approximations of second derivatives. *J. of Comp. Phys.* **199**, 503−540.

Svärd, M., Carpenter, M. H., & Nordström J. 2007 A stable high-Order finite difference scheme for the compressible Navier-Stokes equations, far-field boundary conditions. *J. of Comp. Phys.* **225**, 1020−1038.

Svärd, M. & Nordström, J. 2006 On the order of accuracy for difference approximations of initial-boundary value problems. *J. of Comp. Phys.* **218**, 333−352.

Winckelmans, G., Cocle, R., Dufresne, L., Capart, R., Bricteux, L., Daeninck, G., Lonfils, T., Duponcheel, M., Desenfans, O. & Georges L. 2006 Direct Numerical Simulation and Large-Eddy Simulation of wake vortices: Going from laboratory conditions to flight conditions. *European Conference on Computational Fluid Dynamics, ECCOMAS CFD 2006.*